

Lateral magnetic stiffness under different parameters in a high-temperature superconductor levitation system

Yong Yang(杨勇) and Yun-Yi Wu(吴云翼)

Citation: Chin. Phys. B, 2021, 30 (**7**): 077404. DOI: 10.1088/1674-1056/abe0c2
Journal homepage: http://cpb.iphy.ac.cn; http://iopscience.iop.org/cpb

What follows is a list of articles you may be interested in

Thermal stability and thermoelectric properties of Cd-doped nano-layered Cu_2Se prepared using NaCl flux method

Jianhua Lu(陆建华), Decong Li(李德聪), Wenting Liu(刘文婷), Lanxian Shen(申兰先), Jiali Chen(陈家莉), Wen Ge(葛文), and Shukang Deng(邓书康)
Chin. Phys. B, 2020, 29 (**12**): 127403. DOI: 10.1088/1674-1056/abbbf5

NMR and NQR studies on transition-metal arsenide superconductors $LaRu_2As_2$, $KCa_2Fe_4As_4F_2$, and $A_2Cr_3As_3$

Jun Luo(罗军), Chunguang Wang(王春光) Zhicheng Wang(王志成), Qi Guo(郭琦), Jie Yang(杨杰), Rui Zhou(周睿), K Matano, T Oguchi, Zhian Ren(任治安), Guanghan Cao(曹光旱), Guo-Qing Zheng(郑国庆)
Chin. Phys. B, 2020, 29 (**6**): 067402. DOI: 10.1088/1674-1056/ab892d

Electrochemical synthesis of alkali-intercalated iron selenide superconductors

Shen Shi-Jie, Ying Tian-Ping, Wang Gang, Jin Shi-Feng, Zhang Han, Lin Zhi-Ping, Chen Xiao-Long
Chin. Phys. B, 2015, 24 (**11**): 117406. DOI: 10.1088/1674-1056/24/11/117406

Optimization of intergrain connection in high-temperature superconductor $Bi_2Sr_2CaCu_2O_x$

Li Cheng-Shan, Zhang Sheng-Nan, Hao Qing-Bin, Ma Xiao-Bo, Lu Tian-Ni, Zhang Ping-Xiang
Chin. Phys. B, 2015, 24 (**7**): 077401. DOI: 10.1088/1674-1056/24/7/077401

Crystal chemistry and structural design of iron-based superconductors

Jiang Hao, Sun Yun-Lei, Xu Zhu-An, Cao Guang-Han
Chin. Phys. B, 2013, 22 (**8**): 087410. DOI: 10.1088/1674-1056/22/8/087410

Lateral magnetic stiffness under different parameters in a high-temperature superconductor levitation system*

Yong Yang(杨勇)[1,†] and Yun-Yi Wu(吴云翼)[2,3,‡]

[1] School of Mechano-Electronic Engineering, Xidian University, Xi'an 710071, China
[2] China Three Gorges Science and Technology Research Institute, Beijing 100036, China
[3] Physikalisches Institute B, RWTH Aachen, Aachen 52056, Germany

(Received 30 September 2020; revised manuscript received 9 January 2021; accepted manuscript online 28 January 2021)

Magnetic stiffness determines the stability of a high-temperature superconductor (HTS) magnetic levitation system. The quantitative properties of the physical and geometrical parameters that affect the stiffness of HTS levitation systems should be identified for improving the stiffness by some effective methods. The magnetic stiffness is directly related to the first-order derivative of the magnetic force with respect to the corresponding displacement, which indicates that the effects of the parameters on the stiffness should be different from the relationships between the forces and the same parameters. In this paper, we study the influences of some physical and geometrical parameters, including the strength of the external magnetic field (B_0) produced by a rectangular permanent magnet (PM), critical current density (J_c), the PM-to-HTS area ratio (α), and thickness ratio (β), on the lateral stiffness by using a numerical approach under zero-field cooling (ZFC) and field cooling (FC) conditions. In the first and second passes of the PM, the lateral stiffness at most of lateral positions essentially increases with B_0 increasing and decreases with β increasing in ZFC and FC. The largest lateral stiffness at every lateral position is almost produced by the minimum value of J_c, which is obviously different from the lateral force–J_c relation. The α-dependent lateral stiffness changes with some parameters, which include the cooling conditions of the bulk HTS, lateral displacement, and movement history of the PM. These findings can provide some suggestions for improving the lateral stiffness of the HTS levitation system.

Keywords: high-temperature superconductor, magnetic levitation, lateral stiffness, lateral force

PACS: 74.72.–h, 84.71.Ba, 85.25.Am, 85.70.Rp **DOI:** 10.1088/1674-1056/abe0c2

1. Introduction

The contactless high-temperature superconductor (HTS) magnetic levitation systems have inherent stability and require less complex control strategies and electronics. The HTS levitation system can be used in a linear configuration for transportation[1–3] or in a rotation-symmetric arrangement as axial or radial passive bearings.[4–6] The performance of the HTS levitation system can be improved by increasing the vertical and lateral forces while obtaining sufficient magnetic stiffness and low damping. In this context, there are many experimental and theoretical studies regarding the improvement of the vertical force and lateral force between permanent magnet (PM) and HTS.[7–10] On the other hand, the HTS levitation systems are limited by their low magnetic stiffness in applications when comparing with mechanical or active magnetic bearings.[11–13] The magnetic stiffness is very important, especially in the applications where operating space is limited and stability is the most demanding requirement.[14]

The magnetic stiffness usually can be obtained by the vertical or lateral force curve (including the minor loops)[15–20] or the dynamic properties.[21] Because in the HTS levitation system, the vertical force and the lateral force are both hysteretic, they after the start of vibration are the corresponding forces acting on the minor loops.[18] Therefore, the magnetic stiffness should be calculated from the vertical or lateral force during a minor loop. In addition, the minor loop size has a great effect on the magnetic stiffness.[22–25] The experimental results reported by Hull and Cansiz revealed that the average magnetic stiffness changed monotonically with the minor loop size.[22] We also simulated the average magnetic stiffness of various laterally or vertically sized minor loops changing from 0.1 mm to 2 mm when the PM moved vertically or horizontally above the HTS.[23–25] The calculation results demonstrated that most of the average magnetic stiffness values were intensely influenced by the sizes of the minor loops. In order to avoid the errors caused by different sizes of the minor loops, the approximate value of the magnetic stiffness was obtained using the linearly extrapolating to zero traverse method.[22–25]

Magnetic stiffness is a main parameter for taking into account the stable levitation. Many researchers devoted effort to finding the methods to enhance the stiffness.[13,14,18,26–30] Navau and Sanchez discussed in detail the dependence of the vertical stiffness on different key parameters of the levitation system, such as the superconductor aspect ratio, the relative size of the superconductor–permanent magnet, and the crit-

*Project supported by the National Natural Science Foundation of China (Grant No. 11572232).
†Corresponding author. E-mail: yangyong@xidian.edu.cn
‡Corresponding author. E-mail: wu_yunyi@ctg.com.cn
© 2021 Chinese Physical Society and IOP Publishing Ltd

ical current of the superconductor.[18] Because they considered cylindrical symmetric configuration with only vertical movement, their model could not describe lateral displacement and lateral stiffness. Sotelo *et al.* investigated the potential of adapting a Halbach configuration of the PMs to improve the radial and axial stiffness of thrust bearings.[26] When the height of field cooling was reduced, the radial stiffness and the axial stiffness were both enhanced exponentially, but the load capability decreased exponentially.[14] A multisurface levitation structure, using three ring PMs and one HTS ring, was adopted by Basaran and Sivrioglu to improve the radial stiffness.[28] Kurbatova numerically investigated the sizes and shapes of the PMs and steel elements to quantitatively evaluate the axial and radial stiffness of the two types of HTS bearings with disk and cylindrical superconducting stator.[30] Very recently, Storey *et al.* investigated the geometry of a thrust magnetic bearing, including a conical frustum shaped permanent magnet and matching HTS toroid and puck assembly, to produce the high vertical and lateral stiffness coupled with high levitation force.[13]

Because the magnetic stiffness is directly related to the firstorder derivative of the vertical or lateral force, the dependence of the vertical or lateral stiffness on the physical and geometrical parameters of HTS levitation system is different from the effects of the same parameters on the vertical or lateral force. In fact, some experimental and theoretical studies have revealed some unexpected phenomena for the magnetic stiffness.[25,31] The recent experimental results showed that the radial stiffness was not influenced by the artificial holes in any bulk HTS thickness region and the optimal thickness with the largest radial stiffness was in a range from 6 mm to 12 mm.[31] However, the axial stiffness was almost constant down to 6-mm thickness of the bulk HTS, and then quickly decreased with further thickness declining. Our latest calculations also demonstrated some surprising results.[25] For example, the numerical results showed that the sign switching phenomenon of the vertical stiffness appeared to be related to several parameters, such as the strength of external magnetic field, the critical current density (J_c) of HTS, and the PM-to-HTS area ratio (α). Although many studies have revealed the magnetic stiffness of HTS levitating system, most of the researchers focus on the stiffness properties of the stationary position that is considered as the working point. But our recent studies showed that the vertical stiffness at different vertical distances had different characteristics for one of the parameters.[25] In addition, the dependence of the lateral stiffness on different important parameters of the HTS levitation system has not been studied comprehensively in both experimental or theoretical aspect. In this context, the effects of the key physical and geometrical parameters of the HTS levitation system on the lateral stiffness at different lateral displacements should be studied in detail.

In this paper, a superconducting magnetic levitation system is composed of a cylindrical superconductor and a rectangular PM, which is one of the simplest forms. The effects of the strength of the magnetic field produced by the PM, J_c of the bulk HTS, and the PM-to-HTS area ratio and thickness ratio on the lateral magnetic stiffness are studied under the conditions of zero-field cooling (ZFC) and field cooling (FC). The rest of this paper is organized as follows. The system geometry and the calculation method of the lateral magnetic stiffness are discussed in Section 2, The results of the lateral stiffness under different parameters (such as the external magnetic field strength, J_c of HTS, and the PM-to-HTS area ratio and thickness ratio) are presented and discussed in Section 3. Finally, the conclusions are drawn from the present study in Section 4.

2. Geometry and calculation models

2.1. Geometry model and moving patterns of PM

We consider a cylindrical bulk HTS with radius R and height H_{SC}, and a rectangular PM with length a, width b, and thickness h_{PM} with uniform magnetization along the axis of its thickness direction. B_0 is the strength of the magnetic flux density at the top surface of the rectangular PM. In the paper, we use the size of B_0 to describe the magnetic field strength of the PM. The scheme of the levitation system in ZFC and FC are shown in Figs. 1(a) and 1(b), respectively. We will use rectangular Cartesian coordinates with the coordinate origin located at the top surface center of the bulk HTS. We consider that the bulk HTS is fixed and the PM above the HTS can be moved in the vertical or lateral direction. In the ZFC case, the bulk HTS is cooled from the normal state to the superconducting state when the PM is located at the vertical position of $z_1 = 30$ mm. Then the PM vertically moves towards the bulk HTS until $z = z_0 = 1$ mm. After that, the PM moves in the lateral direction. In the FC case, the bulk HTS is cooled from the normal state to the superconducting state when the PM is located at the vertical position of $z_1 = z_0 = 1$ mm. After that, the PM traverses in the lateral direction.

The PM moves horizontally from $x = 0$ to a positive maximum lateral displacement $x_{max} = 20$ mm, and then reversing to a negative maximum lateral displacement $\bar{x}_{max} = -x_{max} = -20$ mm, and finally returning to the original position $x = 0$. The general movement process is called the lateral major loop. To calculate the lateral stiffness, a series of minor loop traverses (Δx) varying from 0.1 mm to 2 mm is performed. A minor loop can be produced by a PM moving pattern as follows: as the PM moves to a certain horizontal location, it traverses by a small increment along the opposite lateral direction of the major loop, and then returns to its original position. The vertical distance between the PM and the bulk HTS, z_0, remains constant as the PM laterally moves under ZFC and FC.

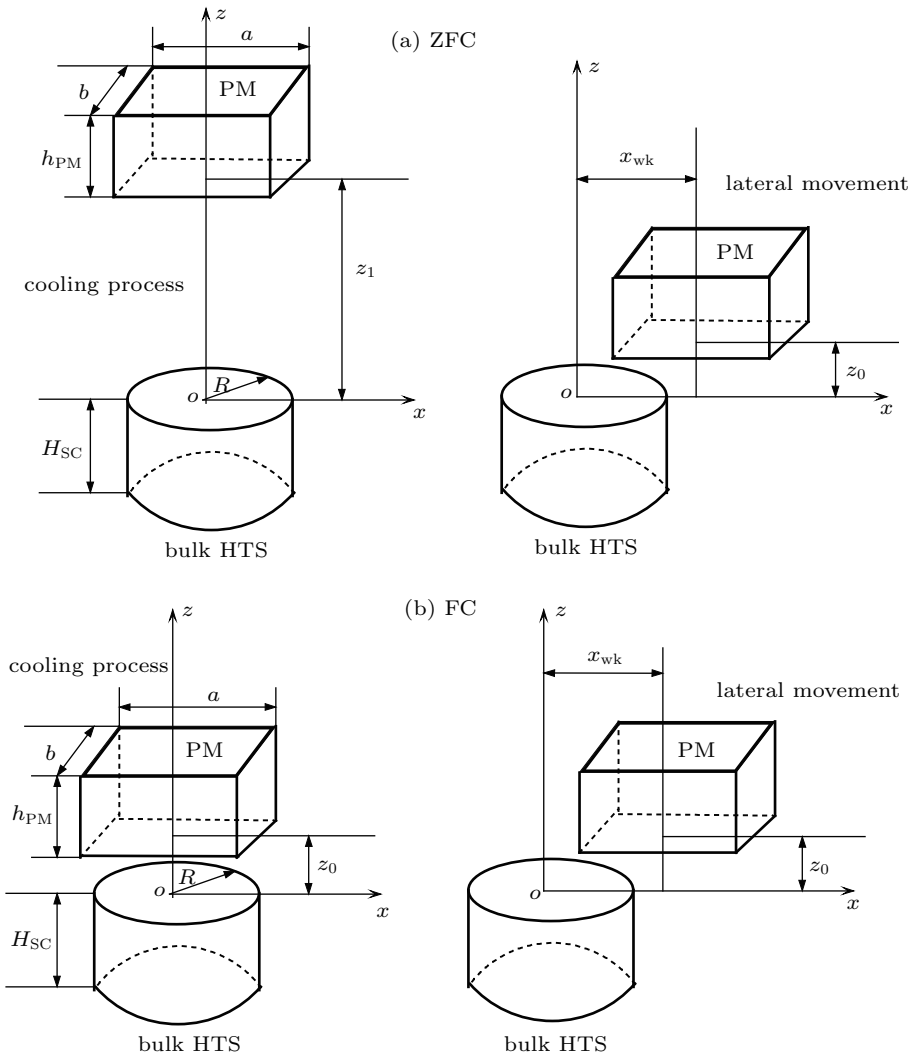


Fig. 1. Geometry and dimensions of considered HTS levitation system under (a) ZFC and (b) FC conditions.

2.2. Calculation method of the lateral stiffness

The shielding current density ($\boldsymbol{J}$) in the bulk HTS can be analyzed by the current vector potential ($\boldsymbol{T}$) method.[32] If the displacement current is ignored and $\boldsymbol{B} = \mu_0 \boldsymbol{H}$ is used, then Ampere's law can be written as

$$\nabla \times \boldsymbol{B} = \mu_0 \boldsymbol{J}, \tag{1}$$

where μ_0 is the magnetic permeability in vacuum, and $\boldsymbol{B}$ and $\boldsymbol{H}$ are the magnetic flux density and magnetic field in HTS, respectively. $\boldsymbol{B}$ can be written as

$$\boldsymbol{B} = \boldsymbol{B}_{\mathrm{e}} + \boldsymbol{B}_{\mathrm{SC}}, \tag{2}$$

where $\boldsymbol{B}_{\mathrm{e}}$ and $\boldsymbol{B}_{\mathrm{SC}}$ are the magnetic flux densities generated by the PM and the shielding current in HTS, respectively.

$\nabla \cdot \boldsymbol{J} = 0$ can be obtained by the operation of divergence on Eq. (1). Accordingly, the current vector potential $\boldsymbol{T}$ can be introduced and defined as $\boldsymbol{J} = \nabla \times T$. The Faraday's law of induction is

$$\nabla \times \boldsymbol{E} = -\frac{\partial \boldsymbol{B}}{\partial t}, \tag{3}$$

where $\boldsymbol{E}$ is electric field strength in HTS. Using Eqs. (2) and (3) and $\boldsymbol{J} = \sigma \boldsymbol{E}$, we obtain

$$\nabla \times \frac{1}{\sigma} \nabla \times \boldsymbol{T} = \frac{\partial (\boldsymbol{B}_{\mathrm{e}} + \boldsymbol{B}_{\mathrm{SC}})}{\partial t}, \tag{4}$$

where σ is the conductivity of HTS.

According to the Helmholtz theorem, the current vector potential $\boldsymbol{T}$ can be written as[25]

$$\begin{aligned} \boldsymbol{T}(\boldsymbol{r},t) = & \frac{1}{4\pi} \iiint \left\{ \left[\nabla' \times \boldsymbol{T}(\boldsymbol{r}',t) \right] \times \nabla' \left(\frac{1}{R} \right) \right\} \mathrm{d}V' \\ & - \frac{1}{4\pi} \oiint \left\{ \left[\boldsymbol{n} \cdot T(\boldsymbol{r}',t) \right] \nabla' \left(\frac{1}{R} \right) \right\} \mathrm{d}S', \end{aligned} \tag{5}$$

where $\boldsymbol{r}$ and $\boldsymbol{r}'$ respectively denote the vector of field point and the vector of source point, R is the distance from the source point to the field point, $\boldsymbol{n}$ is the surface's unit normal vector. $\boldsymbol{B}_{\mathrm{SC}}$ in HTS can be obtained by Biot–Savart's law

$$\boldsymbol{B}_{\mathrm{SC}} = \frac{\mu_0}{4\pi} \iiint \boldsymbol{J}(\boldsymbol{r}',t) \times \nabla' \left(\frac{1}{R} \right) \mathrm{d}V'. \tag{6}$$

Substituting Eqs. (5) and (6) into Eq. (4), the governing equa-

tion of $\boldsymbol{T}$ method is written as[32,33]

$$\nabla\times\frac{1}{\sigma}\nabla\times\boldsymbol{T}(\boldsymbol{r},t)+\mu_0\frac{\partial\boldsymbol{T}(\boldsymbol{r},t)}{\partial t}+\frac{\mu_0}{4\pi}\iint_S\left[\frac{\partial\left(\boldsymbol{T}(\boldsymbol{r}',t)\cdot n\right)}{\partial t}\nabla'\left(\frac{1}{R}\right)\right]\mathrm{d}S'=-\frac{\partial\boldsymbol{B}_\mathrm{e}}{\partial t},\quad(7)$$

where S is the boundary of the bulk HTS. The analytic expression of the magnetic flux density for a rectangular PM can be found in Ref. [34].

A bulk HTS has an obvious layer structure. Previous study also demonstrated that the J_c of the bulk, parallel to the a–b plane, is three times bigger than that parallel to the c axis.[35] On this basis, it can be reasonably considered that the bulk HTS consists of some thin plates along the c axis. The shielding current density $\boldsymbol{J}$ parallel to the thin plates (a–b plane) is taken into account, while the $\boldsymbol{J}$ parallel to the c axis is neglected for each thin layer. Therefore, the three-dimensional equation (7) can be simplified into a two-dimensional (2D) equation. To solve the 2D equation, the Galerkin finite element method (FEM) and the critical state Bean model are used to obtain the distribution of the shielding current density in the HTS thin layers. Then the lateral force acting on the levitating PM can be evaluated from the Lorentz force expression.

In this study, the lateral stiffness at different lateral positions x_wk, which is called the lateral working point, is investigated, and x_wk is selected as 3, 6, 9, 12, −3, −6, −9, and −12 mm. Due to the hysteresis behavior of the bulk HTS, the lateral stiffness at the same x_wk has different values for the first and second passes of the PM. As the PM moves to a given lateral position x_wk, an average lateral stiffness ($\tilde{k}_{xx}$) is determined by producing a minor loop at the point on the lateral force major curve. The $\tilde{k}_{xx}$ equals the negative slope of the minor loop. So we have

$$\tilde{k}_{xx}=-\frac{\Delta F_x^\mathrm{ml}}{\Delta x},\quad(8)$$

where the superscript ml indicates the lateral force on the minor loop.

For each x_wk, a series of minor loops with different lateral sizes is performed. The lateral sizes of the minor loop (Δx) are selected as 0.1, 0.2, 0.4, 0.6, 0.8,1.0, 1.2, 1.4, 1.6, 1.8, and 2.0 mm, respectively. Different sizes of the minor loop can deduce different values of $\tilde{k}_{xx}$. The approximate value with zero traverse for the lateral stiffness is obtained by linear extrapolation. The approximate value is considered as the accurately lateral stiffness (k_{xx}). Numerical data are recorded every 0.01 mm of lateral displacement.

The lateral force without minor loop, obtained by the same calculation method adopted in this paper, is quantitatively compared with the experimental data[22] in our previous paper,[33] showing that the theoretical calculations accord well with the experimental data for all lateral displacements in ZFC and FC, which means that the calculations of the lateral forces with the minor loops in the paper are reliable too. Then, the calculation results of the average and approximate magnetic stiffness are also credible because those values are derived from the minor loops by the simply linear fitting method. In fact, the magnetic stiffness cannot be directly measured. The lateral stiffness can be generally gained in experimental measurements by the following method. The lateral forces on the minor loops with different values of Δx can be measured by the force sensor. All points of a minor loop are fitted with a straight line to find the slope of each minor loop, which in turn provides the average lateral stiffness $\tilde{k}_{xx}$ for a particular Δx. The lateral stiffness k_{xx} is gained by the linear extrapolation by using all average $\tilde{k}_{xx}$ values with different values of Δx.

3. Results and discussion

B_0 is an essential parameter of the PM for the HTS levitation system and describes the magnetization feature and the magnetic field strength produced by the PM. The value of J_c indicates the flux pinning property of HTS and reflects its electric conductivity. J_c limits $\boldsymbol{J}$ in the bulk HTS and affects the levitation ability because the Lorentz force between PM and HTS is produced by $\boldsymbol{J}$ in the bulk HTS and $\boldsymbol{B}_\mathrm{e}$ of the PM. In addition, the relation between the relative size of the PM–HTS and the levitation characteristics can provide the methods to optimize the HTS levitation machines such as superconducting magnetic bearings and maglev trains. In this context, at different values of x_wk, we have systematically studied the dependence of the lateral stiffness k_{xx} on different physical and geometrical parameters of the HTS levitation system such as the external magnetic field strength of the PM, the J_c of bulk HTS and the PM-to-HTS area ratio and thickness ratio. Unless otherwise stated, we adopt the following parameters: $R=15$ mm, $H_\mathrm{SC}=18$ mm, $J_\mathrm{c}=10.0\times10^7$ A/m^2, $a=b=h_\mathrm{pm}=26.58$ mm, and $B_0=0.4$ T. The values of these parameters are generally similar to the ones employed in the previous experimental study.[22] In addition, the values of $R=15$ mm and $a=b=26.58$ mm leads the surface area of the bulk HTS to equal that of the PM. The cylindrical bulk superconductor is divided into nine thin plates along the c axis with each plate being 2-mm thick.

3.1. The B_0 dependence

In order to determine the dependence of k_{xx} on B_0, the other parameters of the HTS levitation system are kept constant as B_0 changes. In ZFC, figures 2(a) and 2(b) show the relationships between k_{xx} and B_0 in the first and second passes of the PM, respectively. The k_{xx} at large lateral displacements (such as $x_\mathrm{wk}=\pm9$ mm and ±12 mm) increases with B_0 increasing from 0.1 T to 0.8 T. Furthermore, at these lateral positions, the k_{xx} increases more rapidly as B_0 increases from

0.4 T to 0.8 T than as B_0 from 0.1 T to 0.4 T. At small lateral displacements (such as $x_{wk} = \pm 3$ and ± 6 mm), the k_{xx} first decreases and then increases as B_0 increases from 0.1 T to 0.8 T. Moreover, in the first pass of the PM, the sign of k_{xx} at some small lateral displacements (such as $x_{wk} = -3$ and ± 6 mm) changes from negative to positive value with B_0 increasing from 0.4 T to 0.8 T (Fig. 2(a)). This means that the lateral stability positioned at the lateral displacements changes from unstable state to stable state as the PM magnetic field becomes strong enough. The phenomenon of sign switching for the k_{xx} also appears at some lateral displacements (such as $x_{wk} = \pm 6$ mm) with B_0 increasing from 0.4 T to 0.8 T in the second pass of the PM (Fig. 2(b)).

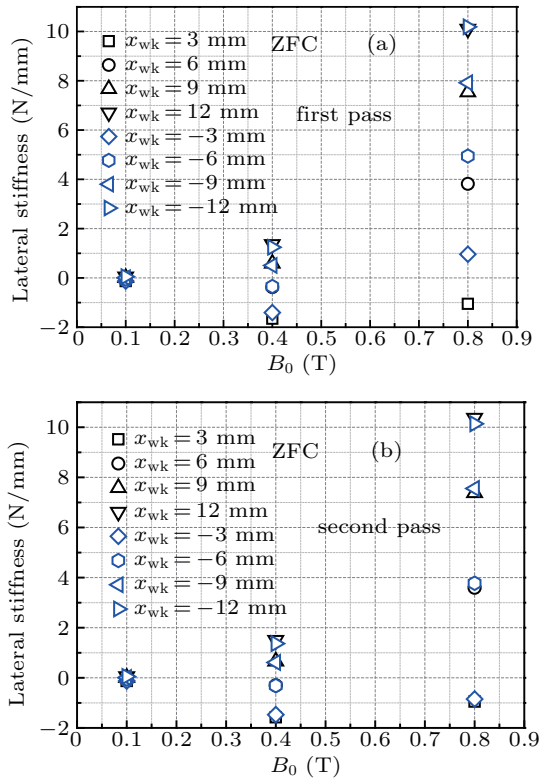


Fig. 2. Relationships between k_{xx} and B_0 at different lateral displacements under the ZFC condition in (a) the first pass and (b) the second pass.

In order to understand the results of k_{xx} with different parameters at different lateral positions, we have plotted the lateral force curves with some minor loops under different values of the parameters. Figure 3 shows the lateral force curves with some minor loops at three different B_0 values in the ZFC case. The lateral size of the minor loop is chosen to be $\Delta x = 0.2$ mm in Fig. 3 because the average lateral stiffness $\tilde{k}_{xx}$ produced by a small minor loop (such as $\Delta x = 0.1$ or 0.2 mm) is usually close to the approximate lateral stiffness k_{xx} based on our previous study.[23] Moreover, the minor loop with $\Delta x = 0.2$ mm is shown more clearly than that with $\Delta x = 0.1$ mm. In Fig. 3, we observe that all minor loops coincide with the major loops with B_0 of 0.1 T and 0.4 T. However, the minor loops are separate from the large loop with a B_0 of 0.8 T due to the strong magnetic hysteresis effect. The $\tilde{k}_{xx}$ with $\Delta x = 0.2$ mm equals the negative value of the slope of the minor loop at a certain x_{wk} if the minor loop is separate from the major loop, or equals the negative value of the derivative at the same x_{wk} when the minor loop coincides with the corresponding major loop. Accordingly, at $x_{wk} = 6$ mm, the $\tilde{k}_{xx}$ with $B_0 = 0.1$ T is close to zero, while has a negative value with $B_0 = 0.4$ T and has a positive value with $B_0 = 0.8$ T. Therefore, the $\tilde{k}_{xx}$ (or k_{xx}) at $x_{wk} = 6$ mm first decreases and then increases as B_0 increases from 0.1 T to 0.8 T. In addition, the sign of k_{xx} switches at $x_{wk} = 6$ mm as B_0 increases from 0.4 T to 0.8 T. This means that since the shape of the lateral force curve varies or the minor loops are separate from the corresponding major loops, the lateral stability at some lateral positions changes from unstable state to stable state when the applied magnetic field becomes strong. At the other lateral positions, the characteristics of k_{xx} can also be understood by the similar analysis about the lateral force curves with the minor loops.

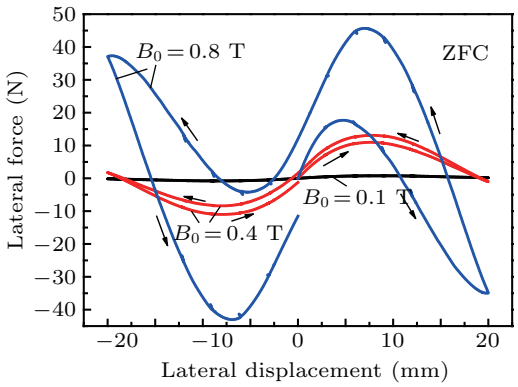


Fig. 3. Lateral forces under different B_0 values with minor loops laterally sized at 0.2 mm under the ZFC condition.

Figures 4(a) and 4(b) show the B_0-dependent k_{xx} values at different lateral positions under FC condition in the first and second passes of the PM, respectively. The k_{xx} at all lateral positions increases with B_0 increasing from 0.1 T to 0.8 T. Furthermore, at each x_{wk}, the k_{xx} increases faster as B_0 increases from 0.4 T to 0.8 T than B_0 increasing from 0.1 T to 0.4 T. The k_{xx} at each x_{wk} value has a positive value under any B_0, which implies that the HTS levitation system is always laterally stable in the FC case with B_0 increasing from 0.1 T to 0.8 T. Figure 5 displays the lateral force curves with some minor loops under three different B_0 values in the FC case. As the external magnetic field produced by the PM becomes strong, the minor loops start to be separate from the major loop with $B_0 = 0.8$ T because of the strong magnetic hysteresis effect. The derivative values of the major lateral force curve at some lateral displacements (generally ranging from -7.5 mm to 7.5 mm) with $B_0 = 0.8$ T become positive values in the second pass of the PM due to the remarkable flux pinning effect. However, the slops of the minor loops have negative values at these lateral positions in the same displacement range. Thus, if the lateral stiffness is deduced from the derivative of the major lateral force curve in the region where the strong magnetic

hysteresis effect appears, the sign of the lateral stiffness may be opposite to that obtained from the slop of the minor loop.

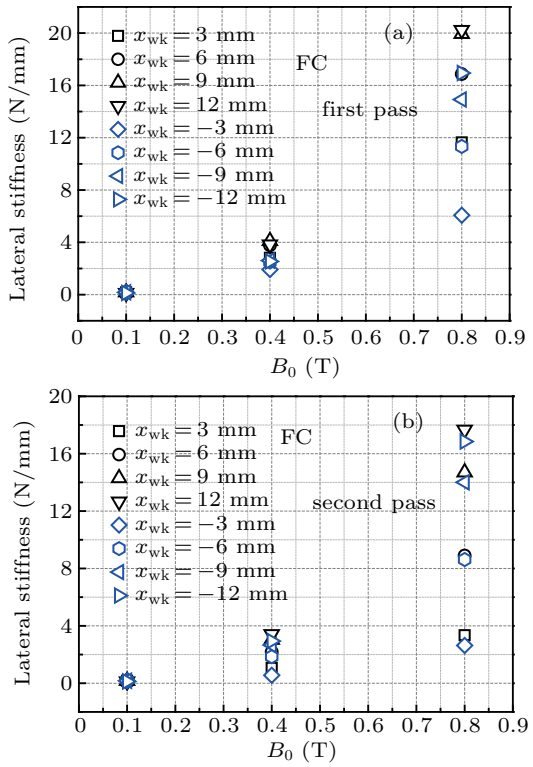


Fig. 4. Relationships between k_{xx} and B_0 at different lateral displacements under the FC condition in (a) the first pass and (b) the second pass.

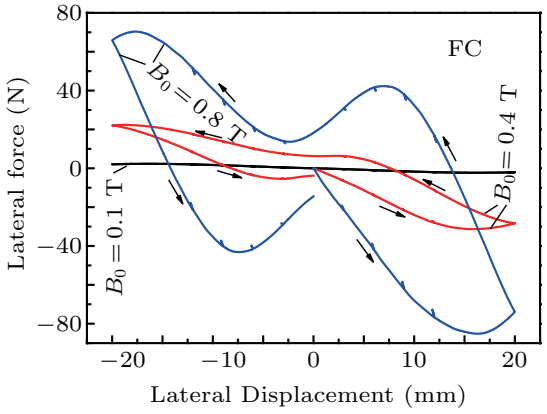


Fig. 5. Lateral forces under different B_0 values with minor loops laterally sized at 0.2 mm in the FC case.

3.2. The J_c dependence

In ZFC, the J_c-dependent k_{xx} values in the first and second passes of the PM are shown in Figs. 6(a) and 6(b), respectively. Figure 7 shows the lateral force curves with some minor loops at three different J_c values in the ZFC case. At each lateral position, the k_{xx} decreases almost linearly as J_c increases from 1.0×10^7 A/m^2 to 10.0×10^7 A/m^2 no matter whether it happens in the first pass or the second pass of the PM. The results of k_{xx} are considerably distinguished from the lateral forces at different J_c values, because the lateral force can be generally enhanced as J_c increases (Fig. 7). The reason is that the minor loops easily deviate from the major loops as J_c decreases from 10.0×10^7 A/m^2 to 1.0×10^7 A/m^2 due to the enhancement of the magnetic hysteresis effect. This means that when the initial cooling height is large (or in the ZFC case), the lateral stability of the levitation system will be significantly enhanced if J_c of the bulk HTS decreases. As shown in Fig. 6, the sign of k_{xx} at small lateral displacements (such as $x_{wk} = \pm3$ mm and ±6 mm) changes from plus to minus as J_c increases from 1.0×10^7 A/m^2 to 10.0×10^7 A/m^2. The reason is that the minor loops tend to coincide with the major loops as J_c increases and the lateral levitation is unstable for a large enough J_c in the ZFC case. In addition, the k_{xx} values at some lateral positions of $x_{wk} = 3$, 6, 9, and 12 mm almost equal those at corresponding symmetrical positions of $x_{wk} = -3$, -6, -9, and -12 mm, respectively. It implies that the k_{xx} has symmetrical characteristic about the axis of $x = 0$ in the ZFC case, where J_c is kept identical.

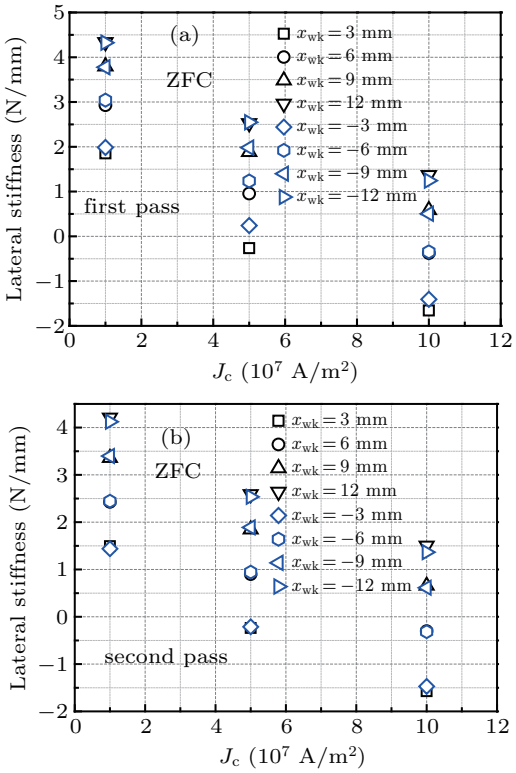


Fig. 6. Values of k_{xx} as a function of J_c at different lateral displacements under the ZFC condition in (a) the first pass and (b) the second pass.

In the FC condition, the J_c-dependent k_{xx} values in the first and second passes of the PM are shown in Figs. 8(a) and 8(b), respectively. Figure 9 shows the lateral force curves with some minor loops at three different J_c values in the FC case. In the first pass of the PM, the k_{xx} at $x_{wk} = 3$ mm or 6 mm slightly changes with J_c increasing from 1.0×10^7 A/m^2 to 10.0×10^7 A/m^2, but the k_{xx} at $x_{wk} = -3$ mm first decreases and then increases for the same change of J_c. The behaviors of k_{xx} can be explained from Fig. 9. Although the derivative increases at $x_{wk} = 3$ mm or 6 mm on the major loop as J_c increases from 1.0×10^7 A/m^2 to 10.0×10^7 A/m^2, the minor loops deviate more evidently from the major loops under

$J_c = 1.0 \times 10^7$ A/m^2 and 5.0×10^7 A/m^2 than that under $J_c = 10.0 \times 10^7$ A/m^2. These changes of the minor loops at the two lateral positions cause the value of k_{xx} to have a small change under the three J_c values in the first pass of the PM. At $x_{wk} = -3$ mm, very minor loop under different J_c values deviates from the corresponding major loop due to the sensitiveness of the bulk HTS to the PM movement history. The largest slope of the minor loops is produced when $J_c = 1.0 \times 10^7$ A/m^2, followed by $J_c = 10.0 \times 10^7$ A/m^2, and the smallest one is produced when $J_c = 5.0 \times 10^7$ A/m^2. Therefore, the k_{xx} at $x_{wk} = -3$ mm first decreases and then increases with J_c increasing from 1.0×10^7 A/m^2 to 10.0×10^7 A/m^2 in the first pass of the PM. At the other lateral positions (such as $x_{wk} = 9$, 12, -6, -9, and -12 mm), the k_{xx} decreases monotonically as J_c increases from 1.0×10^7 A/m^2 to 10.0×10^7 A/m^2.

As shown in Fig. 8(b), in the second pass of the PM, at small lateral displacements (such as $x_{wk} = \pm 3$ mm and ± 6 mm), the k_{xx} significantly decreases as J_c increases from 1.0×10^7 A/m^2 to 5.0×10^7 A/m^2, but it slightly increases or decreases with J_c further increasing. At large lateral displacements (such as $x_{wk} = \pm 9$ mm and ± 12 mm), the k_{xx} almost decreases linearly as J_c increases from 1.0×10^7 A/m^2 to 10.0×10^7 A/m^2. Like the case in the first pass of the PM, the reasons for the k_{xx} results under different J_c values can also be understood by analyzing the slopes of the minor loops in Fig. 9. In addition, as shown in Figs. 8(a) and 8(b), all lateral stiffness values are positive in the two passes of the PM. This means that the lateral levitation of the system is always stable under different J_c values in the FC case.

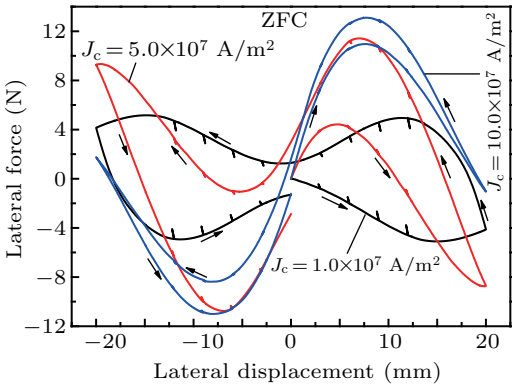


Fig. 7. Lateral forces under different J_c values with minor loops laterally sized at 0.2 mm in the ZFC case.

Although none of the lateral stiffness values at all lateral positions always exhibits the absolute decreasing tendency in the FC case (Fig. 8), the largest lateral stiffness is almost produced by $J_c = 1.0 \times 10^7$ A/m^2 at each x_{wk} whether in the first or in the second pass of the PM when comparing the results of k_{xx} under different J_c values in ZFC (Fig. 6). The calculated results in Figs. 6 and 8 show that as J_c of the bulk HTS becomes large, the k_{xx} at each x_{wk} generally decreases under both the ZFC condition and the FC condition although the lateral force roughly increases (Figs. 7 and 9). This extraordinary phenomenon originates from the case that the minor loops deviate from the major loops, which is caused by the strong magnetic hysteresis effect as J_c decreases.

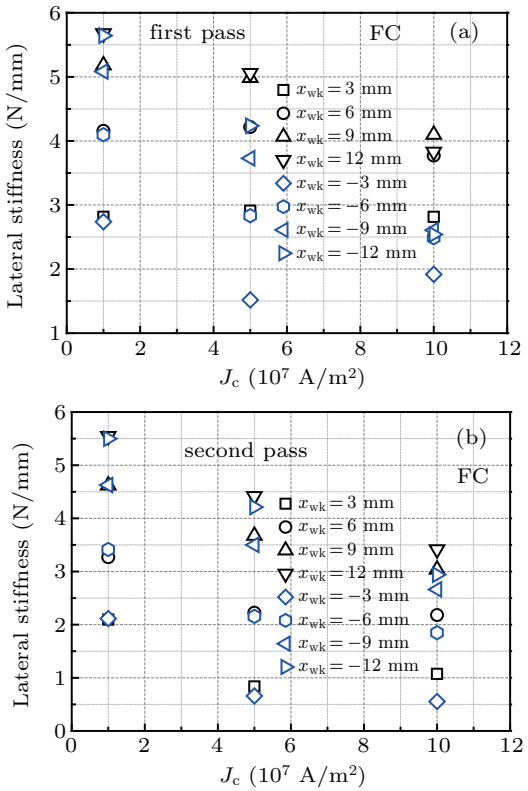


Fig. 8. Values of k_{xx} as a function of J_c at different lateral displacements under the FC condition in (a) the first pass and (b) the second pass.

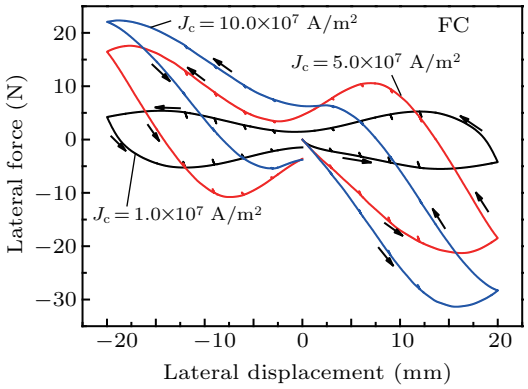


Fig. 9. Lateral forces under different J_c values with minor loops laterally sized at 0.2 mm in the FC case.

3.3. Effect of PM-to-HTS area ratio

Figures 10(a) and 10(b) show the relationships between the calculated k_{xx} and the PMtoHTS area ratio α at different lateral positions under the ZFC condition in the first and second passes of the PM, respectively. The different α values are produced by changing the PM cross-sectional area. As α changes from 0.5 to 2.0, the magnetic pole face of the PM remains square in shape and the dimensions of the bulk HTS remain constant. As α increases from 0.5 to 1.0, the k_{xx} values at different lateral positions display different characteristics. At small lateral displacements (such as $x_{wk} = \pm 3$ mm), the k_{xx} decreases quickly with α increasing from 0.5 to 1.0.

At medium lateral displacements, the k_{xx} slightly decreases (at $x_{wk} = \pm 6$ mm) or increases (at $x_{wk} = \pm 9$ mm) with α increasing from 0.5 to 1.0. However, at large lateral displacements (such as $x_{wk} = \pm 12$ mm), the k_{xx} increases significantly with α increasing from 0.5 to 1.0. The results of k_{xx} can be understood from Fig. 11, where the lateral force curves with some minor loops at three different α values in the ZFC case are plotted. Because all minor loops almost coincide with the corresponding major loops for three different α values, the lateral stiffness at any x_{wk} is generally equal to the negative derivative at the same point on the corresponding major loop. As shown in Fig. 11, since the lateral force curve for $\alpha = 1.0$ is steeper at $x_{wk} = 3$ mm than that for $\alpha = 0.5$, the derivative of the corresponding major loop for $\alpha = 1.0$ is larger than for $\alpha = 0.5$ at the same point whether in the first or in the second pass of the PM. But the lateral stiffness values at $x_{wk} = 3$ mm for $\alpha = 0.5$ and 1.0 are negative. Therefore, the lateral stiffness at the point decreases with α increasing from 0.5 to 1.0. For the other lateral positions, the characteristics of k_{xx} can also be explained by analyzing the shapes of the lateral force curves. As seen from Fig. 10, the k_{xx} at each lateral position decreases with α increasing from 1.0 to 2.0 in the two passes of the PM. Therefore, the k_{xx} value for $\alpha = 1.0$ is the largest in the three α values at $x_{wk} = \pm 12$ mm, but the k_{xx} decreases monotonically at $x_{wk} = \pm 3$ mm as α increases from 0.5 to 2.0. This means that the k_{xx} values with α at different x_{wk} values exhibit the absolutely different features.

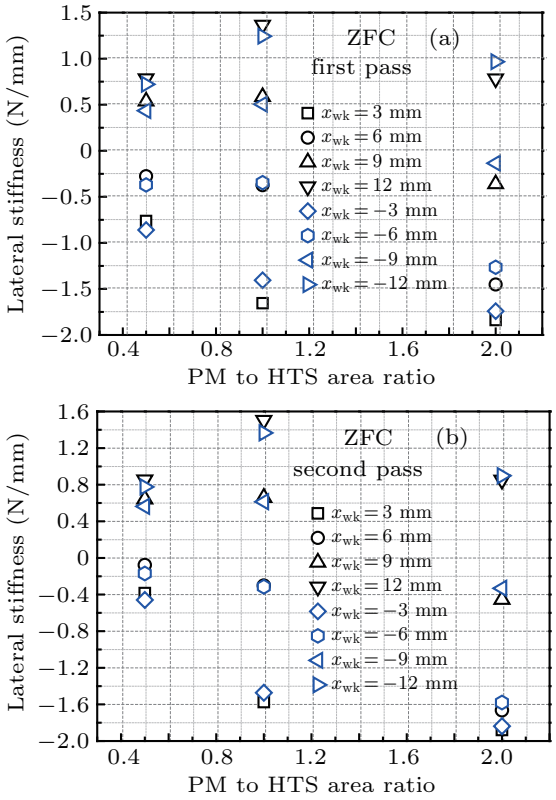


Fig. 10. Relationships between k_{xx} and PM-to-HTS area ratio at different lateral displacements under the ZFC condition in (a) the first pass and (b) the second pass.

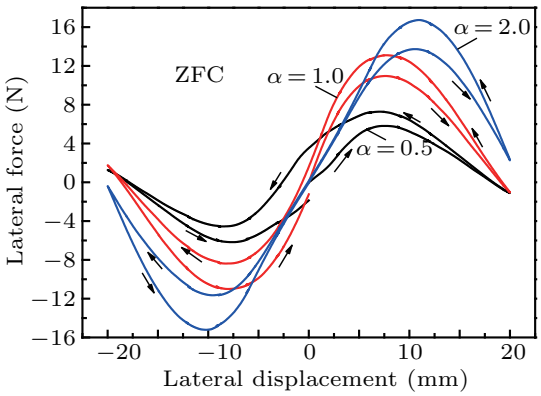


Fig. 11. Lateral forces under different PM-to-HTS area ratios (α) with minor loops laterally sized at 0.2 mm in ZFC.

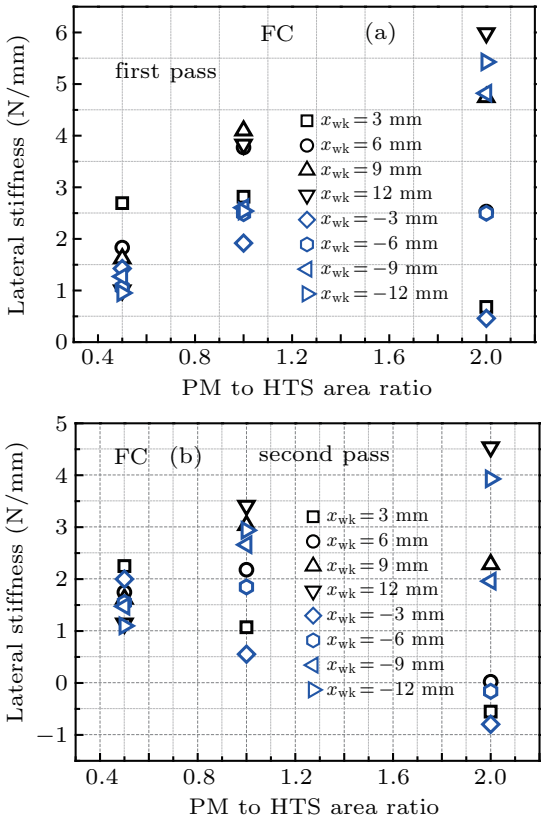


Fig. 12. Relationships between k_{xx} and PM-to-HTS area ratio at different lateral displacements under the FC condition in (a) the first pass and (b) the second pass.

Under the FC condition, the k_{xx} values as a function of α at different lateral positions are shown in Fig. 12. In the first pass of the PM (Fig. 12(a)), the k_{xx} for $\alpha = 1.0$ is generally the largest in the three α values at small lateral displacements (such as $x_{wk} = \pm 3$ mm and ± 6 mm), but the k_{xx} increases monotonically at large lateral displacements (such as $x_{wk} = \pm 9$ mm and ± 12 mm) as α increases from 0.5 to 2.0. In the second pass of the PM (Fig. 12(b)), the k_{xx} for $\alpha = 1.0$ is generally the largest in the three α values at $x_{wk} = \pm 6$ mm and ± 9 mm, but the k_{xx} decreases monotonically at $x_{wk} = \pm 3$ mm and increases monotonically at $x_{wk} = \pm 12$ mm as α increases from 0.5 to 2.0. The different characteristics of k_{xx} in the FC condition can be understood from Fig. 13, which displays the

lateral force curves with some minor loops under different α values. Although all minor loops almost coincide with the corresponding major loops for three different α values, the shapes of the lateral force curves are significantly influenced by α. Like the analysis method under the ZFC case in this section, the above-mentioned features of the lateral stiffness in the FC case can be understood by studying the derivatives at these lateral positions on the major loops for different α values.

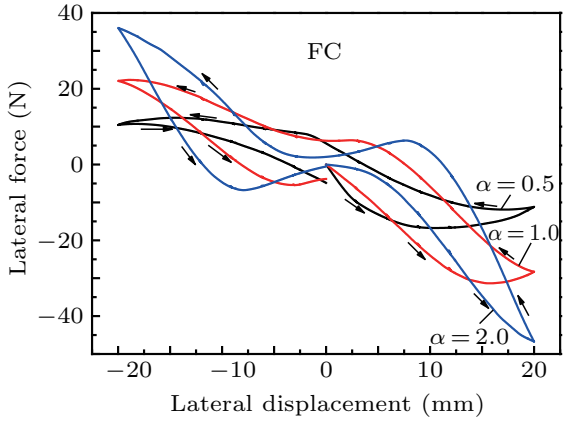


Fig. 13. Lateral forces under different PM-to-HTS area ratio (α) values with minor loops laterally sized at 0.2 mm in FC.

3.4. Effect of PM-to-HTS thickness ratio

In Figs. 14(a) and 14(b), the dependence of k_{xx} on the PMtoHTS thickness ratio ($\beta = h_{\rm PM}/H_{\rm SC}$) under the ZFC condition, in the first and second passes of the PM, is plotted, respectively. The different values of β are obtained by changing the PM thickness, while the dimensions of the bulk HTS remain constant. In addition, the PM surface dimensions and B_0 also remain constant. Whether in the first or in the second pass of the PM, the k_{xx} at each lateral position decreases with β increasing from 0.5 to 2.0. The sign of k_{xx} is always minus at small lateral displacements (such as $x_{\rm wk} = \pm 3$ mm) for different β values, which means that the lateral levitation of the system is unstable at these working points in the ZFC case. However, the sign of k_{xx} always is plus at large lateral displacements (such as $x_{\rm wk} = \pm 9$ mm and ± 12 mm) for any β value. Thus, the system is laterally stable at these positions. At $x_{\rm wk} = \pm 6$ mm, the sign of k_{xx} changes from plus to minus as β increases from 0.5 to 2.0. These phenomena can be understood from Fig. 15, which shows the lateral force curves with some minor loops under different β values in the ZFC case. Owing to the large magnetic hysteresis effect, most of the minor loops are separate from the major loop for $\beta = 0.5$. Although the derivatives of the major loop at $x_{\rm wk} = \pm 6$ mm for $\beta = 0.5$ have positive values, the slopes of the minor loops have negative values because the orientations of the minor loops are different from the tangent lines of the major loop at the same points. Therefore, the lateral stiffness is positive when $x_{\rm wk} = \pm 6$ mm and $\beta = 0.5$. Because the minor loops coincide with the corresponding major loop at $x_{\rm wk} = \pm 6$ mm for $\beta = 2.0$, the lateral stiffness values are deduced from the derivatives of the major loop and have negative values. This leads to the phenomenon of sign switching for the k_{xx} at $x_{\rm wk} = \pm 6$ mm as β increases from 0.5 to 2.0. Obviously, the lateral force curve for $\beta = 0.5$ is the steepest in the three lateral force curves and the minor loops evidently deviate from the large loop for the same β. Thus, the k_{xx} for $\beta = 0.5$ at large displacements (such as $x_{\rm wk} = \pm 9$ mm and ± 12 mm) has the largest values in the three β values.

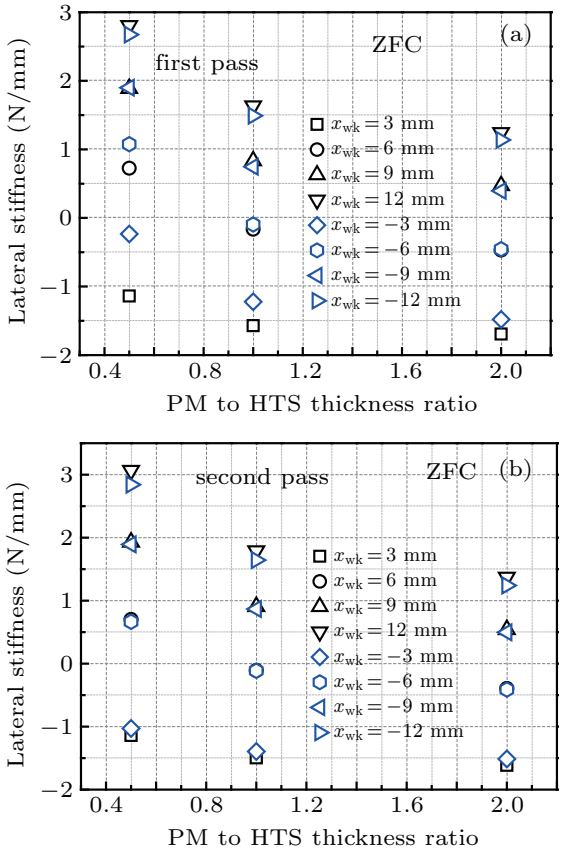


Fig. 14. Values of k_{xx} as a function of PM-to-HTS thickness ratio at different lateral displacements under the ZFC condition in (a) the first pass and (b) the second pass.

Figures 16(a) and 16(b) show the dependence of k_{xx} on β under the FC condition in the first and second passes of the PM, respectively. Like the ZFC case in this section, the k_{xx} at each lateral position also decreases with β increasing from 0.5 to 2.0 whether in the first or in the second pass of the PM. All lateral stiffness values are positive no matter how β and $x_{\rm wk}$ change in the two passes of the PM. This means that the lateral levitation of the system is stable at each $x_{\rm wk}$ for any β value in the FC case. Figure 17 shows the lateral force curves with some minor loops under different β values in the FC case. We observe that the steepest lateral force curve is produced for

$\beta = 0.5$, followed by $\beta = 1.0$, and the last one is produced for $\beta = 2.0$. In addition, the minor loops clearly deviate from the major loop for $\beta = 0.5$. These characteristics of the lateral force curves with the minor loops cause the k_{xx} at each x_{wk} to decrease as β increases from 0.5 to 2.0.

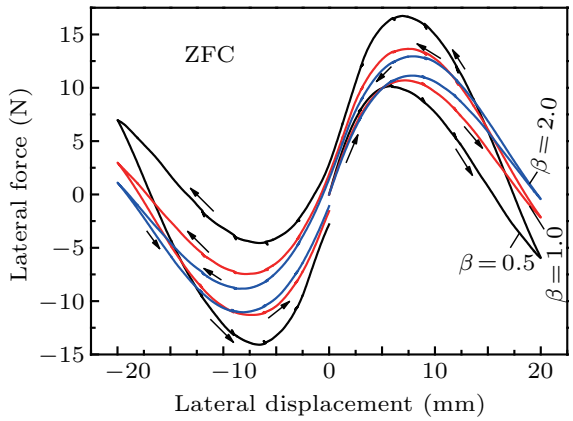


Fig. 15. Lateral forces under different PM-to-HTS thickness ratio (β) values with minor loops laterally sized at 0.2 mm in the ZFC case.

As seen from Figs. 15 and 17, the shape change of the lateral force curve is more obvious as β varies from 0.5 to 1.0 than that as β increases from 1.0 to 2.0. Therefore, the k_{xx} at each lateral position decreases more rapidly when β changes from 0.5 to 1.0 than when β increases from 1.0 to 2.0 (Figs. 14 and 16).

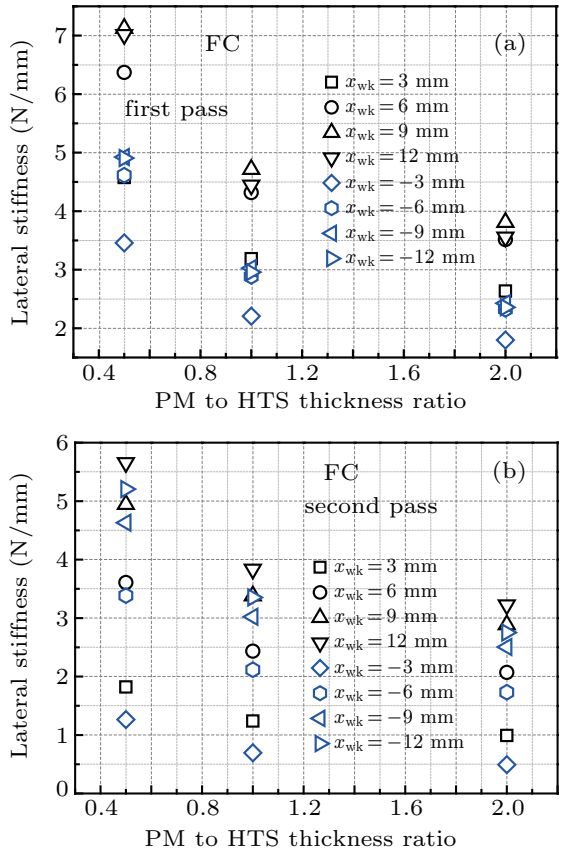


Fig. 16. Values of k_{xx} as a function of PM-to-HTS thickness ratio at different lateral displacements under the FC condition in (a) the first pass and (b) the second pass.

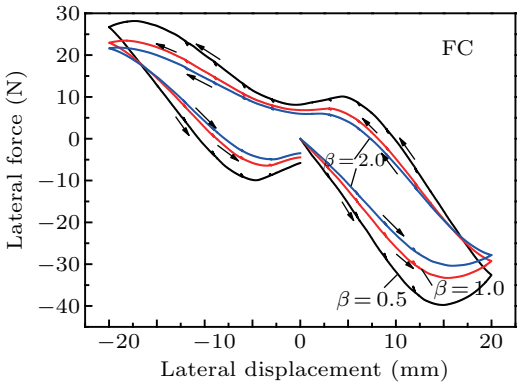


Fig. 17. Lateral forces under different PM-to-HTS thickness ratio (β) values with minor loops laterally sized at 0.2 mm in FC.

4. Conclusions

By using the $\boldsymbol{T}$ method, Bean model, and analytic expressions of the magnetic field produced by a rectangular PM,[34] the lateral force is obtained from an FEM. The average lateral stiffness of a certain minor loop is equal to its negative slope value. The lateral size of the minor loop (Δx) changes from 0.1 mm to 2 mm. By using the linear extrapolation and at the same time by applying all average lateral stiffness values produced by the minor loops with different lateral sizes, the approximate value with a zero traverse for the lateral stiffness is gained. We also study the effects of the B_0 of the PM, J_c, α, and β on the lateral stiffness at different lateral positions in the first and second passes of the PM under ZFC and FC conditions. The conclusions and unexpected results are summarized as follows:

(i) At most lateral positions (except $x_{wk} = \pm 3$ mm and ± 6 mm in the ZFC case), the lateral stiffness increases with the increase of B_0 in the two passes of the PM under the ZFC and FC conditions. In the ZFC case or at relatively high cooling height, the lateral stability at some lateral positions (such as $x_{wk} = \pm 6$ mm) can be changed from unstable state to stable state as the PM magnetic field (in other words, B_0) becomes strong enough.

(ii) In the ZFC case, the lateral stiffness almost decreases linearly with J_c increasing from 1.0×10^7 A/m^2 to 10.0×10^7 A/m^2 at each lateral position whether in the first or in the second pass of the PM. In the FC case, although the lateral stiffness at each lateral position does not always exhibit the absolute decreasing features with J_c increasing, the largest lateral stiffness is generally produced by the minimum value of J_c. The unexpected results indicate that although the lateral force essentially increases, the lateral stiffness decreases as J_c improves.

(iii) The α-dependent lateral stiffness changes with some parameters, which includes cooling conditions of the bulk HTS, lateral displacement, and movement history of the PM.

(iv) In ZFC and FC conditions, the lateral stiffness at each lateral position decreases with β increasing from 0.5 to 2.0

whether in the first or in the second pass of the PM. Moreover, the lateral stiffness decreases more rapidly with β increasing from 0.5 to 1.0 than from 1.0 to 2.0.

References

[1] Bernstein P and Noudem J 2020 *Supercond. Sci. Technol.* **33** 033001
[2] Wang J S, Wang S Y, Zeng Y W, *et al.* 2002 *Physica C* **378–381** 809
[3] Mattos L S, Rodriguez E, Costa F, Sotelo G G, de Andrade R and Stephan R M 2016 *IEEE Trans. Appl. Supercond.* **26** 3600704
[4] Werfel F N, Floegel-Delor U, Rothfeld R, Riedel T, Goebel B, Wippich D and Schirrmeister P 2012 *Supercond. Sci. Technol.* **25** 014007
[5] Ai L W, Zhang G M, Li W J, Liu G L and Liu Q 2018 *Physica C* **550** 57
[6] Miyazaki Y, Mizuno K, Yamashita T, Ogata M, Hasegawa H, Nagashima K, Mukoyama S, Matsuoka T, Nakao K, Horiuch S, Maeda T and Shimizu H 2016 *Cryogenics* **80** 234
[7] Ozturk K, Kabaer M, Abdioglu M, Patel A and Cansiz A 2016 *J. Alloys Compd.* **689** 1076
[8] Bernstein P, Colson L, Dupont L and Noudem J 2017 *Supercond. Sci. Technol.* **30** 065007
[9] Cansiza A, Yildizerb İ and McGuiness D T 2019 *Cryogenics* **98** 60
[10] Zhao B J, Deng Z G, Hu Z X, Liu Y, Zhang S and Zheng J 2020 *IEEE Trans. Appl. Supercond.* **30** 6800305
[11] Ma K B, Postrekhin Y V and Chu W K 2003 *Rev. Sci. Instrum.* **74** 4989
[12] Siems S O and Canders W R 2004 *Supercond. Sci. Technol.* **18** S86
[13] Storey J G, Szmigiel M, Robinson F, Wimbush S C and Badcock R A 2020 *IEEE Trans. Appl. Supercond.* **30** 0600706
[14] Valiente-Blanco I, Diez-Jimenez E, Cristache C, Alvarez-Valenzuela M A and Perez-Diaz J L 2014 *Tribol. Lett.* **54** 213
[15] Moon F C, Yanoviak M M and Ware R 1988 *Appl. Phys. Lett.* **52** 1534
[16] Moon F C, Weng K C and Chang P Z 1989 *J. Appl. Phys.* **66** 5643
[17] Riise A B, Johansen T H, Bratsberg H, Koblischka M R and Shen Y Q 1999 *Phys. Rev. B* **60** 9855
[18] Navau C and Sanchez A 2002 *Supercond. Sci. Technol.* **15** 1445
[19] Valle N D, Sanchez A, Pardo E, Navau C and Chen D X 2007 *Appl. Phys. Lett.* **91** 112507
[20] Ozturk K, Sahin E, Abdioglu M, Kabaer M, Celik S, Yanmaz E and Kucukomeroglu T 2015 *J. Alloys Compd.* **643** 201
[21] Espenhahn T, Wunderwald F, Möller M, Sparing M, Hossain M, Fuchs G, Abdkader A, Cherif C, Nielsch K and Hühne R 2020 *J. Phys. D: Appl. Phys.* **53** 035002
[22] Hull J R and Cansiz A 1999 *J. Appl. Phys.* **86** 6396
[23] Yang Y and Li C S 2017 *AIP Adv.* **7** 105327
[24] Yang Y and Li C S 2017 *AIP Adv.* **7** 125028
[25] Yang Y and Wu Y Y 2020 *J. Appl. Phys.* **128** 053905
[26] Sotelo G, Ferreira A and Rubers de Andrade F 2005 *IEEE Trans. Appl. Supercond.* **15** 2253
[27] Badía-Majós A, Aliaga A, Letosa-Fleta J, Alfonso M M and Roche J P 2015 *IEEE Trans. Appl. Supercond.* **25** 3601810
[28] Basaran S and Sivrioglu S 2017 *Supercond. Sci. Technol.* **30** 035008
[29] Cansiz A and McGuiness D T 2018 *IEEE Trans. Appl. Supercond.* **28** 5201208
[30] Kurbatova E 2018 *IEEE Trans. Appl. Supercond.* **28** 5207704
[31] Antončík F, Lojka M, Hlásek T, Bartůněk V, Valiente-Blanco I, Perez-Diaz J L and Jankovský O 2020 *Supercond. Sci. Technol.* **33** 045010
[32] Takagi T, Hashimoto M, Arita S, Norimatsu S, Sugiura T and Miya K 1990 *IEEE Trans. Magn.* **26** 474
[33] Yang Y and Zheng X J 2008 *Supercond. Sci. Technol.* **21** 015021
[34] Gou X F, Yang Y and Zheng X J 2004 *Appl. Math. Mech. -Engl. Ed.* **25** 297
[35] Murakami M, Gotoh S, Fujimoto H, Yamaguchi K, Koshizuka N and Tanaka S 1991 *Supercond. Sci. Technol.* **4** S43